Journal Pre-proof

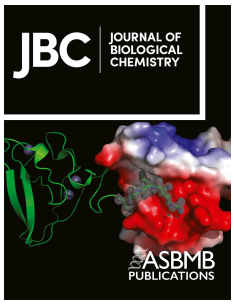

Arsenite oxidase in complex with antimonite and arsenite oxyanions - insights into the catalytic mechanism

Filipa Engrola, Márcia A.S. Correia, Cameron Watson, Carlos C. Romão, Luis F. Veiros, Maria João Romão, Teresa Santos-Silva, Joanne M. Santini

PII: S0021-9258(23)02064-1

DOI: https://doi.org/10.1016/j.jbc.2023.105036

Reference: JBC 105036

To appear in: *Journal of Biological Chemistry*

Received Date: 11 April 2023

Revised Date: 27 June 2023

Accepted Date: 5 July 2023

Please cite this article as: Engrola F, Correia MAS, Watson C, Romão CC, Veiros LF, Romão MJ, Santos-Silva T, Santini JM, Arsenite oxidase in complex with antimonite and arsenite oxyanions - insights into the catalytic mechanism, *Journal of Biological Chemistry* (2023), doi: https://doi.org/10.1016/j.jbc.2023.105036.

This is a PDF file of an article that has undergone enhancements after acceptance, such as the addition of a cover page and metadata, and formatting for readability, but it is not yet the definitive version of record. This version will undergo additional copyediting, typesetting and review before it is published in its final form, but we are providing this version to give early visibility of the article. Please note that, during the production process, errors may be discovered which could affect the content, and all legal disclaimers that apply to the journal pertain.

© 2023 THE AUTHORS. Published by Elsevier Inc on behalf of American Society for Biochemistry and Molecular Biology.

Journal Pre-proof

Arsenite oxidase in complex with antimonite and arsenite oxyanions - insights into the catalytic mechanism

Filipa Engrola[a,b,#], Márcia A. S. Correia[a,b,#], Cameron Watson[c], Carlos C. Romão[d], Luis F. Veiros[e], Maria João Romão[a,b,*], Teresa Santos-Silva[a,b,*], Joanne M. Santini[c,*]

[a] UCIBIO – Applied Molecular Biosciences Unit, Department of Chemistry, School of Science and Technology, NOVA University Lisbon, 2819-516 Caparica, Portugal

[b] Associate Laboratory i4HB - Institute for Health and Bioeconomy, School of Science and Technology, NOVA University Lisbon, 2819-516 Caparica, Portugal

[c] Institute of Structural and Molecular Biology, Division of Biosciences, University College London, WC1E 6BT, United Kingdom

[d] ITQB NOVA, NOVA University Lisbon, Av. da República, 2780-157 Oeiras, Portugal

[e] Centro de Química Estrutural, Institute of Molecular Sciences, Departamento de Engenharia Química, Instituto Superior Técnico, Universidade de Lisboa, Av. Rovisco Pais, 1049 001 Lisboa, Portugal

*corresponding authors (mjr@fct.unl.pt; tsss@fct.unl.pt; j.santini@ucl.ac.uk)

[#] both authors contributed equally to this work

Journal Pre-proof

ABSTRACT

Arsenic contamination of groundwater is among one of the biggest health threats affecting millions of people in the world. There is an urgent need for efficient arsenic biosensors where the use of arsenic metabolizing enzymes can be explored. In this work we have solved the crystal structures of four complexes of arsenite oxidase (Aio) obtained in complex with arsenic and antimony oxyanions and the structures determined correspond to intermediate states of the enzymatic mechanism. These structural data were complemented with DFT calculations providing a unique view of the molybdenum active site at different time points that, together with mutagenesis data, enabled to clarify the enzymatic mechanism and the molecular determinants for the oxidation of As(III) to the less toxic As(V) species.

Keywords: arsenite oxidase, enzyme mechanism, DFT calculations, X-ray crystallography, molybdenum enzyme, arsenic, antimony.

Journal Pre-proof

Introduction

Arsenic and antimony are two metalloids that, due to anthropogenic and natural causes [1,2], pose an environmental threat, and are considered by the World Health Organization as priority pollutants. Maximum drinking-water recommended levels (10 ppb As, 20 ppb Sb) [3] are exceeded in many places throughout the planet with no remediation solution simultaneously effective, clean, and economically sustainable [4-7]. Chemically, both elements share numerous similarities: in aqueous solution oxidation states III and V are the most common, speciating as oxyanions of arsenite/antimonite ($As^{III}(OH)_3/Sb^{III}(OH)_3$), thermodynamically favored in anoxic environments, and

Journal Pre-proof

arsenate/antimonate ($[As^{V}(OH)_2O_2]^-$/$[Sb^{V}(OH)_2O_2]^-$/$[Sb^{V}(OH)_6]^-$), favored under oxygenated conditions [8-10]. Both elements have relatively high redox potentials, $E^{0\prime}$ +140 mV and +94 mV for As^{III}/As^{V} and Sb^{III}/Sb^{V}, respectively, which explains the existence of both oxidized and reduced forms in environmental and biological conditions [11,12]. The reduced forms of As and Sb are harder to remove from soils and water and are considered more toxic to living organisms than the oxidized ones [8,11].

Arsenite oxidase (Aio), is an ancient bioenergetic enzyme present in microbes since the early stages of life on Earth, with its origin dated prior to the evolutionary split of Archaea and Bacteria [13]. Widespread among prokaryotes, it has been identified in 78 different bacterial strains [14,15], and purified from several microorganisms [16-21]. The Aio from *Pseudorhizobium banfieldiae* str. NT-26 (previously *Rhizobium* sp. str. NT-26) (NT-26 Aio) has been tested as a biosensor for arsenite [22,23] but optimization is required.

Aio belongs to the DMSO reductase (DMSOR) family of molybdopterin (Moco)-dependent enzymes, with the Mo atom coordinated by two molybdopterin guanine dinucleotides (MGD) [24]. The enzyme catalyzes the 2-electron oxidation of As^{III} as well as of Sb^{III}, albeit with pronounced differences in reaction kinetics: Sb^{III} salts are oxidized around 6500 times slower than the corresponding As^{III} salt [21,25].

To date, the only 3D structures available are those from NT-26 Aio (PDB 4AAY/5NQD) and from *Alcaligenes faecalis* Aio (*Af* Aio) (PDB 1G8K/1G8J) [26-28]. The enzymes differ in terms of their quaternary structures (Figure S1) but exhibit overall similar structures despite only 48% sequence identity; they superimpose with RMSD of 1.84 Å for Cα of 948 matching residues. The large subunit, AioA, contains the catalytic Moco and one [3Fe-4S] cluster, while the smaller subunit, AioB, harbors a Rieske [2Fe-2S] cluster [28]. Aio is unique when compared to other members of the DMSOR family:

i) the Mo ion is not coordinated to an amino acid side chain; ii) according to crystallographic and extended X-ray absorption fine structure (EXAFS) data, Mo is bound to one/two oxo ligand(s) in addition to the two MGD dithiolenes; and iii) it harbors a [3Fe-4S] and a Rieske cluster, instead of the typical [4Fe-4S] and/or [2Fe-2S] clusters (Figure 1). The unusual features of this enzyme and its importance in bioremediation/biosensing aroused the interest of the scientific community in the last two decades [29-32]. A proposed mechanism of arsenite oxidation at the Mo center was suggested based on the X-ray structures of the free enzyme, cyclic voltammetry, EXAFS and Density Functional Theory (DFT) calculations [26,27,32,33]. To further clarify how arsenite and antimonite are oxidized, we solved and analyzed the crystal structures of functionally relevant As/Sb complexes of NT-26 Aio and *Af* Aio. These data were integrated with site directed mutagenesis and DFT calculations, allowing us to disclose the catalytic mechanism of Aio and the structural determinants, paving the way for future biotechnological applications.

Results and discussion

Overall structures of Aio-oxyanion complexes and the catalytic pocket

Four Aio-oxyanion complexes were obtained using different crystallization conditions and soaking protocols, varying the soaking time and the substrate - arsenite and antimonite salts, after enzyme activation with potassium ferricyanide [33] (crystallization details in Table S1). The high-resolution data (Table S2) revealed unusual coordination modes of As/Sb to the Moco center, corresponding to putative reaction intermediates. As in the published free structures (4AAY, 5NQD and 1G8K [26-28]), the four NT-26 and *Af* Aio complexes crystallized as a dimer of heterodimers ($[\alpha\beta]_2$) (Figure S1, Table S3) with overall structures very similar to the free forms. In all protein-ligand

Journal Pre-proof

complexes, the Moco active site is at the bottom of a hydrophilic funnel-like cavity and the Mo atom adopts a five or six-coordinated geometry: 4 sulfur atoms from the two MGD dithiolenes, and one or two oxo-ligands, in a square pyramidal or a trigonal prismatic geometry, respectively (Figure 1).

In all structures, the presence of As or Sb at the enzyme active site is unambiguous, directly interacting with Mo *via* bridging oxygens (Figures 2,3). At the second coordination sphere, are several highly conserved residues: Asp169, His199, Arg201, Glu207, Lys413, Arg447, His451, Glu453 (NT-26 Aio numbering). Some of these residues (His199, Glu207, Arg447, His451) have been suggested as pivotal for catalysis [26,27,34] since they form direct hydrogen bonds with the Mo=O ligand (Figure 2) while others interact with the substrate via a conserved network of water molecules. The two acidic residues Asp169 and Glu453 are located at the entrance of the highly solvated substrate funnel that leads to the Mo site and their mutation to alanine, resulted in a decrease of specific activity of 30 and 65 %, respectively (Table S4; Figure 2). Both residues are not H-bonded to residues of the catalytic site, only to water molecules that in turn, make H-bonds with the Sb/As-oxyanions bound to Moco. These residues sit at *ca* 4.2 Å from O2 and O3 atoms and >5 Å from Sb (NT-26 Aio-Sb_d; Figure 2c for reference). Since these residues are located at the entrance of the substrate tunnel, they are more exposed to solvent than those closer to the active site, as can be seen by the solvent-accessible surface area (SASA) (Table S5 [82]). Residue Asp169 has a SASA of >250 $Å^2$ and Glu453 of >280 $Å^2$, considerably larger than His451, at the first coordination sphere of Mo, SASA of *ca* 140 $Å^2$ (see Figure 2c for reference). This indicates that, although these residues do not contact directly with the As/Sb ligands, they influence catalysis by stabilizing water molecules conserved in all structures determined that interact with the substrates through H-bonds (conserved in all structures determined).

Interestingly, three water molecules found in the free *Af* Aio structure (1G8K) occupy the substrate-binding site as previously anticipated by Ellis [27] (Figure 2).

Although As and Sb have been refined with partial occupancy, the corresponding B factors are in the same range as those of surrounding atoms (occupancy refinement was done iteratively using Refmac and Phenix software and by visual inspection $2F_o$-F_c, F_o-F_c, and anomalous difference Fourier maps and B factors; Table S6). The variation in occupancy of the As/Sb atoms in the structures can possibly be explained by differences in the crystallization, soaking conditions and dynamics of the reaction. It is known that the solubility, and thus, availability of As^{III} and Sb^{III} ions in sodium arsenite and antimonyl tartrate salts, are pH dependent, hence influenced by the different crystallization solutions used [36]. Also, diffusion through the crystal channels is a limiting factor for reactivity and not all available catalytic sites are equally exposed in the crystal matrix. The four refined structures are now described individually. It should be stressed that, as expected, the 4 Aioα polypeptide chains (A, C, E, G) present slight variability in bond distances at the active sites (Tables S7 and S8) but a clear pattern is observed in the different cases.

Structure of *Af* Aio-As_c

In this structure the As ion is bound to Mo *via* one μ-oxo bridge (Mo-Ox-As), and coordinated to two other oxo/hydroxo groups (O1 and O2) (Figures 3-A and 4 and Figure S3 showcasing anomalous map). The oxygen Ox shared by Mo and As is apical to Mo, at 1.7 Å from Mo and 1.7-1.8 Å from As (distance range in the 4 molecules of the asymmetric unit (AU) (Table S7)). In this structure the Mo is pentacoordinated and the As and Mo ions are 3.3 Å apart, in agreement with NT- 26 Aio-As EXAFS data [33]. In

Af Aio-As_c the As atom is not apical to Mo and the Mo-O-As bond is not linear but bent (about 140º) with the AsO_3 group slightly over the MGD-P dithiolene (Figure 3-A).

Structures of NT-26 Aio-Sb_d and *Af* Aio-As_d

In these structures the Mo atom is *cis* coordinated to two oxygen atoms (O1 and Ox), shared with As/Sb (Figures 3-B,C). The Mo-O single bond distances are ~2 Å (varying 1.77 - 2.29 Å in the 4 molecules of the AU (Table S7)). In both structures the As/Sb atoms are sitting vertically to the Mo dithiolene plane, at ~ 3.1 Å for the As-Aio complex and ~3.3 Å for the Sb-Aio complex (Figure 3; Tables S7, S8) and equidistant to the two pterins: the four dithiolene sulfur atoms are at 4.5-4.8 Å from As and 4.6-5.2 Å from Sb. The bond lengths within the As/Sb oxyanions (As/Sb to O1, Ox, O2, O3, and O4) are very similar in the 4 molecules (Table S7). The crystal structure of a polyoxometalate containing μ-oxo bridged Sb and Mo (CSD YORPUS [35]) (Figure S2) shows a similar geometry and bond distances as the intermediate structure (NT-26 Aio-Sb_d) now reported.

Structure of *Af* Aio-Sb_e

In this structure the Sb atom is sitting vertically to Mo and coordinated to the oxo ligand (Mo-Ox-Sb) and to four additional oxo/hydroxo groups (O1, O2, O3 and O4) (Figure 3-D). Sb-O distances are ~2 Å and Sb is ~3.5 Å from the Mo (Table S6), closer to the MGD-P dithiolene. In contrast to the Aio_d intermediates, where the two bridging oxygens (O1 and Ox) are equidistant to Mo, in Aio-Sb_e, the Mo-O1 distance is too long to be considered a covalent bond (range 2.6 - 3.2 Å, Table S7). In this case as in structure *Af* Aio-As_c, Mo is pentacoordinated, adopting a trigonal prismatic geometry.

Journal Pre-proof

DFT calculations and reaction mechanism

So far, all ligand-free crystal structures of Aio show a single oxo group coordinated to the Mo atom (structure (f) in Figure 5) probably resulting from X-ray photoreduction (to Mo^{IV}), while the oxidized enzyme is proposed to have a di-oxo/hydroxo Mo coordination (Mo^{VI}) (Figure 5, structure (a)) [27]. Considering the structures of the captured reaction intermediate forms here described, we suggest that the reaction cycle (Figure 5) starts by a nucleophilic attack of the substrate arsenite to the oxidized 6-coordinated Mo (Mo^{VI}), specifically *via* the non-spectator oxo ligand (O1, step I). This corresponds to the first step in the DFT calculated reaction profile [37], from **A** to **C** with a barrier of 24 kcal/mol (Figure 4-A).

The reaction proceeds with the As/Sb atoms moving apical to Mo from **C** to **C'** in the profile of Figure 4A (Figure 5, step II). Interestingly, a structure with two symmetrical μ-oxo bridges (**H**) such as observed in the X-ray structures (d) (NT-26 Aio-Sb_d and *Af* Aio-As_d) is readily obtained from intermediate **C'** with a barrier of 11 kcal/mol (Figure 4B, **H**). The μ-oxo bridges stabilize the substrate in the active site, enabling the oxo-transfer step, in which Mo-O1 bond is broken, giving rise to a single oxo coordinated Mo (Figure 5 step V and structure (f), and **E** in Figure 4A profile). This is a facile step with a calculated barrier of merely 3 kcal/mol (from **C'** to **D**, in Figure 4A). The product displacement results in free arsenate/antimonate and a reduced Mo, with a single-oxo coordination, (Mo^{IV}=O/-OH). The addition of a water molecule and the concurrent transfer of two electrons and two protons to the iron-sulfur clusters regenerates the Mo^{VI} dioxo form and restarts the catalytic cycle (step I). This corresponds to the last part of the profile (Figure 4A), from **E** back to **A**, and has a 19 kcal/mol barrier for water coordination. Considering the DFT calculations, the intermediate structure (c) (*Af* Aio-

As_c) is not present along the mechanism and, thus, we have interpreted it as a side product and/or a dead-end structure.

Conclusion

This work contributes to the clarification of the enzymatic reaction mechanism of the oxidation of As(III) to the less toxic As(V) revealing for the first time atomic resolution structures of putative intermediates bearing different As/Sb anions bound to the Mo active site. The Aio enzymatic mechanism relies on the formation of two symmetrical μ-oxo bridges, present in the oxidation of As(III) as well as of Sb(III). The oxyanions are held in the active site pocket by covalent bonding to the Mo cofactor as well as by an intricate network of H bonds with water molecules and charged side chains. In fact, site directed mutagenesis revealed that 2 conserved acidic residues involved in this network are essential for catalysis even though they are located at the entrance of the catalytic funnel, at *ca* 8 Å from the Mo ion. The intermediate species here found are good evidence that reaction mechanisms often proposed based solely on theoretical calculations correspond to a simplification of the various states that arise during an enzymatic reaction, enlightening the importance of experimental structural data. This study provides atomic resolution data on a complex metalloprotein, combining crystallography, mutagenesis and *in silico* calculations. The elucidation of the catalytic mechanism and the knowledge of the molecular determinants for catalysis is vital in the design of new and improved arsenite oxidases with higher stability and substrate specificity. These unique enzymes are very suitable candidates for biotechnological applications for the development of biosensors for As(III/V) and Sb(III/V) using

Journal Pre-proof

engineered enzymes as well as for bioremediation of these toxic species, where robust and reliable systems are still lacking [29,31,38-40].

Journal Pre-proof

Experimental Procedures

Heterologous expression and purification of *Af* Aio and of NT-26 Aio – wild type and D169A and E453A mutants

Expression of NT-26 and of *Af* Aio was done aerobically in *E. coli* DH5α cells at 21 ºC, for 24 h in Luria Broth (LB) media, containing 40 μM of isopropyl β-D-1-thiogalactopyranoside (IPTG); in the case of NT-26 Aio mutants, *E. coli* Tuner cells were used and 250 μM of IPTG was required for overexpression. The enzymes were purified using Ni^{2+}-affinity, and in the case of NT-26 Aio WT, an additional step of size exclusion chromatography was carried out to increase enzyme purity, as previously described [25,27]. The protein was concentrated in 50 mM Tris pH 7.8, up to 20 $mg.mL^{-1}$, and stored at 4 ºC.

Crystallization and preparation of complexes of NT-26 Aio and *Af* Aio

Wild type enzymes were crystallized using the sitting drop vapour diffusion method. For NT-26 Aio, the crystallization drops were prepared using a ratio of 2 μl of protein and 1 μl of reservoir solution with 2M ammonium sulphate as precipitant, 0.1 M Hepes pH 7.5 and 2% (v/v) polyethylene glycol (PEG) 400 (no mixing), as reported [28]; in contrast, crystals of *Af* Aio were obtained using a 1 μl of protein and 1 μl of reservoir solution, using PEG-based conditions that differ from the published one [27] regarding pH and the presence of additives (Table S1; also, in this case, precipitant and protein solution were not mixed). For both NT-26 and *Af* Aio proteins, the best crystals appeared at 4 ºC, as thin brownish plates, that grew to their maximum size (*ca* 0.2 x 0.2 x 0.05 mm) within approximately 2 weeks.

To obtain protein-ligand complexes, crystals were first soaked in a harvesting buffer (HB) containing a slightly higher concentration of the precipitating agent (ammonium sulphate for NT-26 Aio and PEG for *Af* Aio) – increment of 2% (v/v) – and

Journal Pre-proof

50 mM $K_3[Fe(CN)_6]$ to oxidize the protein. Afterwards, crystals were soaked in HBs containing 10 mM of one of the two substrates - potassium antimonyl tartrate trihydrate (Sb^{III}) or sodium arsenite (As^{III}) -using different soaking times (Table S1). The catalytic reaction was stopped upon flash-freezing the crystals in liquid nitrogen, having 20 % (v/v) glycerol as cryoprotectant.

X-ray data collection and structure determination

Diffraction data were collected at PXIII of the Swiss Light Source (SLS, Villigen, Switzerland), at Biomax, MAX IV (Lund, Sweden) and at XALOC, ALBA (Barcelona, Spain). The NT-26 Aio and the *Af* Aio crystals, soaked with As or Sb salts, diffracted to high resolution (ranging from 1.89 to 1.44 Å for the different complexes – see Table S2 for details). Data were processed using the XDS and STARANISO program packages [41,42]. Data quality was analyzed using Aimless from the CCP4 package suite [43,44], and structure determination was accomplished by molecular replacement using the ligand-free crystal structure of NT-26 Aio (PDB 5NQD [28]) and *Af* Aio (PDB 1G8K [27]) as search models. Interactive cycles of model building, and refinement were performed with COOT [45], Refmac5 [46] and PHENIX software [47]. To mitigate model bias and overfitting, the ligands were placed only on the latter stage of refinement, looking at the $2F_o$-F_c, F_o-F_c and anomalous difference Fourier maps. Data collection and refinement statistics are shown in Table S2.

Activity assays of NT-26 Aio wild type *vs* mutants D169A and E453

The NT-26 wild type Aio and the D169A and E453A mutants were previously oxidized for 10 minutes with 10 mM potassium ferricyanide, and the excess of the oxidizing agent was removed using a PD-10 desalting column (GE Healthcare), according to the manufacturer's instructions, with 50 mM MES pH 5.5 serving as the elution buffer.

Journal Pre-proof

The reactions were monitored at 600 nm following the reduction of the artificial electron acceptor 2,6-Dichlorophenolindophenol (DCPIP, considering $\Delta\varepsilon_{red\text{-}ox(600nm)}$ of 8.2 $mM^{-1}.cm^{-1}$) [48], using $Na_3As^{III}O_3$ at 2.5 mM, as the substrate. The results corresponding to 3 replicates for each protein (wild type and mutants) are shown in Table S4.

DFT Calculations

All calculations were performed using the GAUSSIAN 09 software package [49] Geometry optimizations were obtained using the PBE0 functional without symmetry constraints and a basis set (b1) consisting of the Stuttgart/Dresden ECP (SDD) basis set [50-52] to describe the electrons of Mo and As, with one *f*-polarization added for Mo [53] and one *d*-polarization function added for As [54-59]; a standard 6-31G(d,p) basis set [53] was used for all other atoms. The PBE0 functional uses a hybrid generalized gradient approximation (GGA), including 25% mixture of Hartree-Fock [60] exchange with DFT [61] exchange-correlation, given by Perdew, Burke and Ernzerhof functional (PBE) [62-64]**.** Transition state optimizations were performed with the Synchronous Transit-Guided Quasi-Newton Method (STQN) developed by Schlegel *et al* [65,66] following extensive searches of the Potential Energy Surface. Frequency calculations were performed to confirm the nature of the stationary points, yielding one imaginary frequency for the transition states and none for the minima. Each transition state was further confirmed by following its vibrational mode downhill on both sides and obtaining the minima presented on the energy profiles. The electronic energies (E_{b1}) were converted to free energy at 298.15 K and 1 atm (G_{b1}) by using zero-point energy and thermal energy corrections based on structural and vibration frequency data calculated at the same level.

Single point energy calculations were performed on the geometries obtained at the PBE0/b1 level using the M06 functional, the same basis for Mo and As and a 6-311++G(d,p) basis set [67-76] for the rest of the elements (basis b2). The M06 functional

is a hybrid meta-GGA functional developed by Truhlar and Zhao [77]**,** and it was shown to perform very well for the kinetics of transition metal molecules, providing a good description of weak and long-range interactions [78,79]. The free energy values presented (G_{b2}) were derived from the electronic energy values obtained at the M06/b2//PBE0/b1 level (E_{b2}) according to the following expression: $G_{b2} = E_{b2} + G_{b1} - E_{b1}$.

Solvent effects (water) were considered in all calculations (including geometry optimizations) using the Polarizable Continuum Model (PCM) initially devised by Tomasi and coworkers [80-84] with radii and non-electrostatic terms of the SMD solvation model, developed by Truhler *et al* [85].

The molybdopterin cofactor was replaced by a simplified dithiolate model in the calculations, for computational expediency. That model reproduces the pyran ring framework observed in the real molybdopterin cofactor (Figure S4).

Data availability

Data supporting this article are included within the main text and supporting information.

Atomic coordinates and structure factors for the crystal structures, have been deposited at the Protein Data Bank (PDB), with the accession numbers: *Af* Aio-As_c: PDB ID 8CFF; NT-26 Aio-Sb_d: PDB ID 8CCQ; *Af* Aio-As_d: PDB ID 8CH9; *Af* Aio-Sb_e: PDB ID 8CGS.

Supporting information

Detailed information about protein production, activity assays, crystallization, and further structural analysis, as well as DFT calculations, is available as Supporting Information.

Acknowledgements

CW is supported by a Biotechnology and Biological Sciences Research Council (BBSRC) Industrial CASE Studentship (BB/L01615X/1) with Bio Nano Consulting Ltd. as the industrial partner. Work supported by UCIBIO funding from FCT-MCTES (UIDB/04378/2020, UIDP/04378/2020, and Engrola PhD student grant UI/BD/151155/2021) and the Institute for Health and Bioeconomy—i4HB (project LA/P/0140/2020). Centro de Química Estrutural (CQE) and Institute of Molecular Sciences (IMS) acknowledge the financial support of FCT-MCTES (Projects UIDB/00100/2020, UIDP/00100/2020, and LA/P/0056/2020, respectively). The authors thank Doctor Pedro Matias for valuable discussions and acknowledge MAX IV Laboratory for time on Beamline Biomax under Proposal [ID20190007]. Research conducted at MAX IV, is supported by the Swedish Research council under contract 2018-07152, the Swedish Governmental Agency for Innovation Systems under contract 2018-04969, and Formas under contract 2019-02496. We also acknowledge the Paul Scherrer Institut, Villigen, Switzerland for synchrotron radiation beamtime at beamline PXIII of the SLS. Some measurements were performed at XALOC beamline at ALBA Synchrotron with the collaboration of ALBA staff.

Authors contributions

FE and MASC contributed equally; FE, MASC, MJR, TSS contributed to protein production, X-ray experiments and structural analysis; CCR and LFV contributed to

discussions on the mechanistic proposal and DFT calculations; MJR, TSS and JMS coordinated the work and all authors contributed to write the manuscript.

Notes

The authors declare that they have no conflicts of interest with the contents of this article.

Journal Pre-proof

References

1. Mandal, B. K., Suzuki, K. T. (2002) Arsenic Round the World: a Review. *Talanta* **58**, 201–235

2. Herath, I., Vithanage, M., Bundschuh, J. (2017) Antimony as a global dilemma: Geochemistry, mobility, fate and transport. *Environ Pollut*, **223**, 545-559

3. Guidelines for drinking-water quality: fourth edition incorporating the first and second addenda (2022) Geneva: World Health Organization. Licence: CC BY-NC-SA 3.0 IGO

4. Singh, R., Singh, S., Parihar, P., Singh, V. P., Prasad, S. M. (2015) Arsenic Contamination, Consequences and Remediation Techniques: A Review. *Ecotoxicol. Environ. Saf*. **112**, 247–270

5. Li, J., Zheng, B. H., He, Y., Zhou, Y., Chen, X., Ruan, S., Yang, Y., Dai, C., Tang, L. (2018) Antimony Contamination, Consequences and Removal Techniques: A Review. *Ecotoxicol. Environ. Saf*. **156**, 125–134

6. Filella, M., Belzile, N., Chen, Y. W. (2002) Antimony in the Environment: A Review Focused on Natural Waters II. *Earth-Sci. Rev*. **59**(1–4), 265–285

7. Podgorski, J., Berg, M. (2020) Global threat of arsenic in groundwater. *Science* **368**(6493),845-850

8. Sharma, V. K., Sohn, M. (2009) Aquatic Arsenic: Toxicity, Speciation, Transformations, and Remediation. *Environ. Int*. **35**(4), 743–759

9. Ropp R. C. (2013) Encyclopedia of the Alkaline Earth Compounds Group 15 (N, P, As, Sb and Bi). In: Alkaline Earth Compounds. Elsevier, pp 199–350

10. Li, J., Zheng, B. H., He, Y., Zhou, Y., Chen, X., Ruan, S., Yang, Y., Dai, C., Tang, L. (2018) Antimony Contamination, Consequences and Removal Techniques: A Review. *Ecotoxicol and Environ Saf*. **156**, 125–134

11. Abin, C. A., Hollibaugh, J. T. (2014) Dissimilatory Antimonate Reduction and Production of Antimony Trioxide Microcrystals by a Novel Microorganism. *Environ Sci Technol.* **48**(1), 681–688

12. Van Hue, N. (2015) Bioremediation of Arsenic Toxicity. In: Chakrabarty N (eds) Arsenic Toxicity: Prevention and Treatment. CRC Press pp 155–166

13. Lebrun, E., Brugna, M., Baymann, F., Muller, D., Lièvremont, D., Lett, M. C., Nitschke, W. (2003) Arsenite Oxidase, an Ancient Bioenergetic Enzyme. *Mol Biol Evol.* **20**(5), 686–693

14. Pal, S., Sengupta, K. (2021) In silico analysis of phylogeny, structure, and function of arsenite oxidase from unculturable microbiome of arsenic contaminated soil. *J Genet Eng Biotechnol*. **19**(1), 47

15. Kaixiang, S., Wang, Q., Wang, G. (2020) Microbial Oxidation of Arsenite: Regulation, Chemotaxis, Phosphate Metabolism and Energy Generation. *Front. Microbiol*. 11, 569282

16. Vanden Hoven, R. N., Santini, J. M. (2004) Arsenite Oxidation by the Heterotroph Hydrogenophaga sp. str. NT-14: The Arsenite Oxidase and Its Physiological Electron Acceptor. *Biochim Biophys Acta.* **1656**(2–3),148–155

17. Teoh, W. K., Salleh, F. M., Shahir, S. (2017) Characterization of Thiomonas delicata Arsenite Oxidase Expressed in Escherichia coli. *3 Biotech* **7**(2), 97

18. Osborne, T. H., Heath, M. D., Martin, A., Pankowski, J. A., Hudson-Edwards, K. A., Santini, J. M. (2013) Cold-Adapted Arsenite Oxidase from a Psychrotolerant Polaromonas Species. *Metallomics* **5**(4), 318–324

19. Prasad, K. S., Subramanian, V., Paul, J. (2009) Purification and Characterization of Arsenite Oxidase from Arthrobacter sp. *BioMetals* **22**(5), 711–721

20. Lieutaud, A., Lis, R. V., Duval, S., Capowiez, L., Muller, D., Lebrun, R., Lignon, S., Fardeau, M. L., Lett, M. C., Nitschke, W., et al (2010) Arsenite Oxidase from Ralstonia sp. 22: Characterization of the Enzyme and Its Interaction with Soluble Cytochromes. *J Biol Chem.* **285**(27), 20433–20441

21. Santini, J. M., Sly, L. I., Schnagl, R. D., Macy, J. M. (2000) A New Chemolithoautotrophic Arsenite-Oxidizing Bacterium Isolated. *Appl Env Microbiol*. **66**(1), 92–97

Journal Pre-proof

22. Male, K. B., Hrapovic, S., Santini, J. M., Luong, J.H.T. (2007) Biosensor for Arsenite Using Arsenite Oxidase and Multiwalled Carbon Nanotube Modified Electrodes. *Anal Chem*. **79**(20), 7831–7837

23. Cass, A. E. G., Johnson, C. J., Santini, J. M. Modified arsenite oxidase and a biosensor for detecting arsenite. Patent WO 2013/057515 Al, 2018

24. Romão, M. J. (2009) Molybdenum and tungsten enzymes: a crystallographic and mechanistic overview. *Dalton Trans*. **21**, 4053-4068

25. Wang, Q., Warelow, T., Kang, Y.S., Romano, C., Osborne, T. H., Lehr, C. R., Bothner, B., McDermott, T.R., Santini, J. M., Wang, G. (2015) Arsenite Oxidase Also Functions as an Antimonite Oxidase. *Appl Environ Microbiol*. **81**(6), 1959–1965

26. Warelow, T., Oke, M., Schoepp-Cothenet, B., Dahl, J. U., Bruselat, N., Sivalingam, G. N., Leimkühler, S., Thalassinos, K., Kappler, U., Naismith, J. H., et al. (2013) The Respiratory Arsenite Oxidase: Structure and the Role of Residues Surrounding the Rieske Cluster. *PLoS One*. **8**(8):e72535

27. Ellis, P. J., Conrads, T., Hille, R., Kuhn, P. (2001) Crystal Structure of the 100 kDa Arsenite Oxidase from Alcaligenes faecalis in Two Crystal Forms at 1.64 Å and 2.03 Å. *Structure* **9**(2), 125-132

28. Watson, C., Niks, D., Hille, R., Vieira, M., Schoepp-Cothenet, B., Marques, A. T., Romão, M. J., Santos-Silva, T., Santini, J. M. (2017) Electron Transfer through Arsenite Oxidase: Insights into Rieske Interaction with Cytochrome c. *Biochim. Biophys. Acta – Bioenerg*. **1858**(10), 865–872

29. Bertin, P. N., Simona, C., Plewniak, F., *et al*. (2022) Water and soil contaminated by arsenic: the use of microorganisms and plants in bioremediation. *Environ Sci Pollut R.* **29**, 9462–9489

30. Kaur, H., Kumar, R., Babu, J. N., Mittal, S. (2015) Advances in arsenic biosensor development – A comprehensive review. *Biosens Bioelectron*. **63**, 533–545

31. Hare, V., Chowdhary, P., Singh, A. K. (2020) Arsenic toxicity: adverse effect and recent advance in microbes mediated bioremediation. In: Microorganisms for Sustainable Environment and Health, pp 53–80

32. Hoke, K. R., Cobb, N., Armstrong, F. A., Hille, R. (2004) Electrochemical Studies of Arsenite Oxidase: An Unusual Example of a Highly Cooperative Two-Electron Molybdenum Center. *Biochemistry* **43**(6), 1667–1674

33. Warelow, T., Pushie, M. J., Cotelesage, J., Santini, J. M., George, G. (2017) The Active Site Structure and Catalytic Mechanism of Arsenite Oxidase. *Sci. Rep.* **7**(1), 1757

34. McNellis, L., Anderson, G.L. (1998) Redox-State Dependent Chemical Inactivation of Arsenite Oxidase. *J Inorg Biochem*. **69**(4), 253–257

35. Bouallegui, T., Harchani, A., Dege, N., Haddad, A., Ayed, B. (2018) Synthesis, characterization, Hirschfeld surface and theoretical properties of a new non-centrosymmetric inorganic/organic material: $(C_7H_{12}N_2)_7(\beta\text{-}SbMo_6O_{24})_2\cdot 8H_2O$. *J Mol Struct.* **1166**, 195-201

36. Kang, M., Kawasaki, M., Tamada, S., Kamei, T., Magara, Y. (2000) Effect of pH on the removal of arsenic and antimony using reverse osmosis membranes. *Desalination*, **131**(1-3), 293–298

37. Parr, R.G., Yang, W. (1989) Density Functional Theory of Atoms and Molecules; Oxford University Press: New York

38. Laha, A., Sengupta, S., Bhattacharya, P., Mandal, J., Bhattacharyya, S., Bhattacharyya, K. (2002) Recent advances in the bioremediation of arsenic-contaminated soils: a mini review. *World J Microbiol Biotechnology*. **38**(11), 189

39. Diba, F., Khan, M., Uddin, S., Istiaq, A., Shuvo, M., Alam, A., Hossain, M., Sultana, M. (2021) Bioaccumulation and detoxification of trivalent arsenic by Achromobacter xylosoxidans BHW-15 and electrochemical detection of its transformation efficiency. *Sci. Rep*. **11**, 21312

40. González-Benítez, N., Durante-Rodríguez, G., Kumar, M., Carmona, M. (2021) Editorial: Biotechnology for Arsenic Detection and Bioremediation. *Front Microbiol.* **12**, 743109

41. Kabsch, W. (2010) XDS. *Acta Crystallogr D Biol Crystallogr*. **66**(Pt 2), 125–132

42. Tickle, I. J., Flensburg, C., Keller, P., Paciorek, W., Sharff, A., Vonrhein, C., Bricogne, G. (2018) STARANISO. Cambridge, United Kingdom: Global Phasing Ltd

43. Evans, P. (2006) Scaling and assessment of data quality. *Acta Crystallogr D Biol Crystallogr*. **62**, 72–82

44. Dodson, E., Winn, M., Ralph, A. (1997) Collaborative computational project, number 4: providing programs for protein crystallography. *Methods Enzymol* **227**, 620–633

45. Emsley, P., Cowtan, K. (2004) Coot: model-building tools for molecular graphics, *Acta Crystallogr D Biol Crystallogr*. **60**, 2126–2132

46. Murshudov, G., Skubak, P., Lebedev, A., Vagin, A. (2011) REFMAC5 for the refinement of Macromolecular Crystal Structures. *Acta Crystallogr D Biol Crystallogr*. **67**(4), 355-67

47. Adams, P. D., Afonine, P.V., Bunkóczi, G., Chen, V.B., Echols, N., Headd, J., Hung, W., Jain, S., Kapral, G.J., Grosse Kunstleve, R.W., McCoy, A., Moriarty, W., Oeffner, D., Read, J., Richardson, C., Richardson, S., Terwilliger, C., Zwart, H. (2011) The Phenix software for automated determination of macromolecular structures. *Methods*. **55**(1), 94–106

48. Armstrong, J. M. (1964) The molar extinction coefficient of 2,6-dichlorophenol indophenol. *Biochim Biophys Acta.* **86**, 194–197

49. Frisch, M. J., Trucks, G. W., Schlegel, H. B., Scuseria, G. E., Robb, M. A., *et al.* (2009) Gaussian 09, Revision A.01. Gaussian, Inc., Wallingford CT

50. Haeusermann, U., Dolg, M., Stoll, H., Preuss, H., Schwerdtfeger, P., Pitzer, R. M. (1993) Accuracy of energy-adjusted quasirelativistic ab initio pseudopotentials. *Mol Phys*. **78**, 1211-1224.

51. Kuechle, W., Dolg, M., Stoll, H., Preuss, H. (1994) Energy-adjusted pseudopotentials for the actinides. Parameter sets and test calculations for thorium and thorium monoxide. *J Chem Phys.* **100**(10), 7535-7542.

52. Leininger, T., Nicklass, A., Stoll, H., Dolg, M., Schwerdtfeger, P. (1996) The accuracy of the pseudopotential approximation. II. A comparison of various core sizes for indium pseudopotentials in calculations for spectroscopic constants of InH, InF, and InCl. *J Chem Phys*. **105**, 1052-1059

53. Ehlers AW, Böhme M, Dapprich S, Gobbi A, Höllwarth A, Jonas V, Köhler KF, Stegmann R, Veldkamp A, Frenking G (1993) A set of f-polarization functions for pseudo-potential basis sets of the transition metals Sc−Cu, Y−Ag and La−Au. *Chem Phys Lett*. **208**,111-114

54. Höllwarth, A., Böhme, M., Dapprich, S., Ehlers, A.W., Gobbi, A., Jonas, V., Köhler, K.F., Stegmann, R., Veldkamp, A., Frenking, G. (1993) A set of d-polarization functions for pseudo-potential basis sets of the main group elements Al-Bi and f-type polarization functions for Zn, Cd, Hg. *Chem Phys Lett*. **208**, 237-240

55. Ditchfield, R., Hehre, W.J., Pople, J.A. (1971) Self-Consistent Molecular-Orbital Methods. IX. An Extended Gaussian-Type Basis for Molecular-Orbital Studies of Organic Molecules. *J Chem Phys* **54**, 724-728

56. Hehre, W.J., Ditchfield, R., Pople, J.A. (1972) Self-Consistent Molecular Orbital Methods. 12. Further extensions of Gaussian-type basis sets for use in molecular-orbital studies of organic-molecules. *J Chem Phys*. **56**, 2257-2261

57. Hariharan, P.C., Pople, J.A. (1974) Accuracy of AH equilibrium geometries by single determinant molecular-orbital theory. *Mol Phys.* **27**, 209-214

58. Gordon, M.S. (1980) The isomers of silacyclopropane. *Chem Phys Lett*. **76**, 163-168

59. Hariharan, P.C., Pople, J.A. (1973) Influence of polarization functions on molecular-orbital hydrogenation energies. *Theor. Chim. Acta,* **28**, 213-222

60. Hehre, W.J., Radom, L., Schleyer, P.R., Pople, J.A. (1986) Ab Initio Molecular Orbital Theory, John Wiley & Sons, NY

61. Parr, R.G., Yang, W. (1989) Density Functional Theory of Atoms and Molecules. Oxford University Press: New York

62. Perdew, J.P., Burke, K., Ernzerhof, M. (1996) Generalized Gradient Approximation Made Simple. *Phys Rev Lett.* **77**, 3865-3868

63. Perdew, J.P., Burke, K., Ernzerhof, M. (1997) Generalized Gradient Approximation Made Simple *Phys Rev Lett*. **78**, 1396-1396

64. Perdew, J.P. (1986) Density-functional approximation for the correlation energy of the inhomogeneous electron gas. *Phys Rev B.* **33**, 8822-8824

65. Peng, C., Ayala, P.Y., Schlegel, H.B., Frisch, M.J. (1996) Using redundant internal coordinates to optimize equilibrium geometries and transition states *J Comp Chem*. **17**, 49-56

66. Peng, C., Schlegel, H.B. (1993) Combining Synchronous Transit and Quasi-Newton Methods for Finding Transition States Israel. *J. Chem.* **33**, 449-454

67. McClean, A.D., Chandler, G.S. (1980) Contracted Gaussian basis sets for molecular calculations. I. Second row atoms, Z=11-18 J. *Chem Phys.* **72**, 5639-5648

68. Krishnan, R., Binkley, J.S., Seeger, R., Pople, J.A. (1980) Self-consistent molecular orbital methods. XX. A basis set for correlated wave functions. *J Chem Phys*. **72**, 650-654

69. Wachters, A.J. H. (1970) Gaussian Basis Set for Molecular Wavefunctions Containing Third-Row Atoms. *J Chem Phys*. **52**, 1033-1036

70. Hay, P.J. (1977) Gaussian basis sets for molecular calculations - representation of 3D orbitals in transition-metal atoms. *J Chem Phys.* **66**, 4377-4384

71. Raghavachari, K., Trucks, G.W. (1989) Highly correlated systems: Excitation energies of first row transition metals Sc-Cu. *J Chem Phys.* **91**, 1062-1065

72. Binning Jr., R.C., Curtiss, L.A. (1990) Compact contracted basis-sets for 3rd-row atoms - Ga-Kr. *J Comp Chem.* **11**, 1206-1216

73. McGrath, M. P., Radom, L. (1991) Extension of Gaussian-1 (G1) theory to bromine-containing molecules. *J Chem Phys.* **94**, 511-516

74. Curtiss, L.A., McGrath, M.P., Blaudeau, J.P., Davis, N.E., Binning Jr., R.C., Radom, L. (1995) Extension of Gaussian-2 theory to molecules containing third-row atoms Ga-Kr. *J Chem Phys*. **103**, 6104-6113

75. Clark, T., Chandrasekhar, J., Spitznagel, G.W., Schleyer, P.R. (1983) Efficient diffuse function-augmented basis-sets for anion calculations. 3. The 3-21+G basis set for 1st-row elements, Li-F. *J. Comp. Chem*. **4**, 294-301

76. Frisch, M.J., Pople, J.A., Binkley, J.S.(1984) Self-Consistent Molecular Orbital Methods. 25. Supplementary Functions for Gaussian Basis Sets. *J Chem Phys.* **80**, 3265-3269

77. Zhao, Y., Truhlar, D.G. (2008) The M06 suite of density functionals for main group thermochemistry, thermochemical kinetics, noncovalent interactions, excited states, and transition elements: two new functionals and systematic testing of four M06-class functionals and 12 other functionals. *Theor. Chem. Acc*. **120**, 215-241

78. Zhao, Y., Truhlar, D.G. (2008) Density Functionals with Broad Applicability in Chemistry. *Acc. Chem. Res.* **41**, 157-167

79. Zhao, Y., Truhlar, D.G. (2011) Applications and validations of the Minnesota density functionals. *Chem Phys Lett.* **502**, 1-13

80. Cancès, M.T., Mennucci, B., Tomasi, J. (1997) A new integral equation formalism for the polarizable continuum model: Theoretical background and applications to isotropic and anistropic dielectrics. *J. Chem. Phys.* **107**, 3032-3041

81. Cossi, M., Barone, V., Mennucci, B., Tomasi, J. (1998) Ab initio study of ionic solutions by a polarizable continuum dielectric model. *Chem. Phys. Lett*. **286**, 253-260

82. DeLano, W.L. (2002) Pymol: An open-source molecular graphics tool. *CCP4 Newsletter On Protein Crystallography.* **40**, 82-89

83. Mennucci, B., Tomasi, J. (1997) Continuum solvation models: A new approach to the problem of solute's charge distribution and cavity boundaries. *J. Chem. Phys*. **106**, 5151-5158

84. Tomasi, J., Mennucci, B., Cammi, R. (2005) Quantum mechanical continuum solvation models. *Chem. Rev.* **105**, 2999-3094

85. Marenich, A.V., Cramer, C.J., Truhlar, D.G. (2009) Universal solvation model based on solute electron density and a continuum model of the solvent defined by the bulk dielectric constant and atomic surface tensions. *J Phys Chem. B*, **113**, 6378-6396

Journal Pre-proof

Figure Captions:

Figure 1. Structure of A) *Af* Aio (PDB ID 1G8K [27]) and B) NT-26 Aio (PDB ID 5NQD [28]) enzymes highlighting the Moco and the iron-sulfur cluster cofactors. AioA subunit harbors the Moco cofactor - with Mo bound to one/two oxo ligand(s), in addition to the two MGD dithiolenes – and a [3Fe-4S] cluster (*Af* AioA in pink and NT-26 AioA in green). AioB subunit harbors a Rieske iron-sulfur center (*Af* AioA in grey and NT-26 AioA in white).

Figure 2. Close-up of the active site of the free (A,C), Sb-complexed (B,E) and As-complexed (D,F) forms of Aio: **A) NT-26 Aio** (chain C) (PDB ID 4AAY), 2.7 Å resolution [26]; **B) NT-26 Aio-Sb_d** (chain E), 1.84 Å resolution; **C) *Af* Aio** (chain A) (PDB ID 1G8K), 1.64 Å resolution [27]; **D) *Af* Aio-As_d** (chain E), 1.44 Å resolution; **E) *Af* Aio-Sb_e** (chain A), 1.84 Å resolution; **F) *Af* Aio-As_c** (chain E), 1.57 Å resolution. Images were prepared using PyMOL [82].

Figure 3. Close up of the *Af* Aio and NT-26 Aio active sites in complex to As/Sb ligands: **A) *Af* Aio-As_c** (chain E), 1.57 Å resolution; **B) *Af* Aio-As_d (**chain E), 1.44 Å resolution; **C) NT-26 Aio-Sb_d** (chain A), 1.84 Å resolution; **D) *Af* Aio-Sb_e** (chain E), 1.84 Å resolution. $2F_o$-F_c map contoured at 1σ. Distances are in Å. Images were prepared using PyMOL software [82].

Figure 4. A) DFT calculated fee energy profile (kcal/mol) for the $As(OH)_3$ oxidation reaction; **B)** conversion between μ1- and μ2-oxo bridged arsenate intermediates. Free energy values (kcal/mol) relative to A. Distances in Å.

Figure 5. Proposed reaction mechanism with crystal structures of intermediate complexes of Aio-ligand (c, d and e) from this work and of the Aio free structure (1G8K [27]) (f). Numbers in parenthesis correspond to the resolution of the diffraction data.

Journal Pre-proof

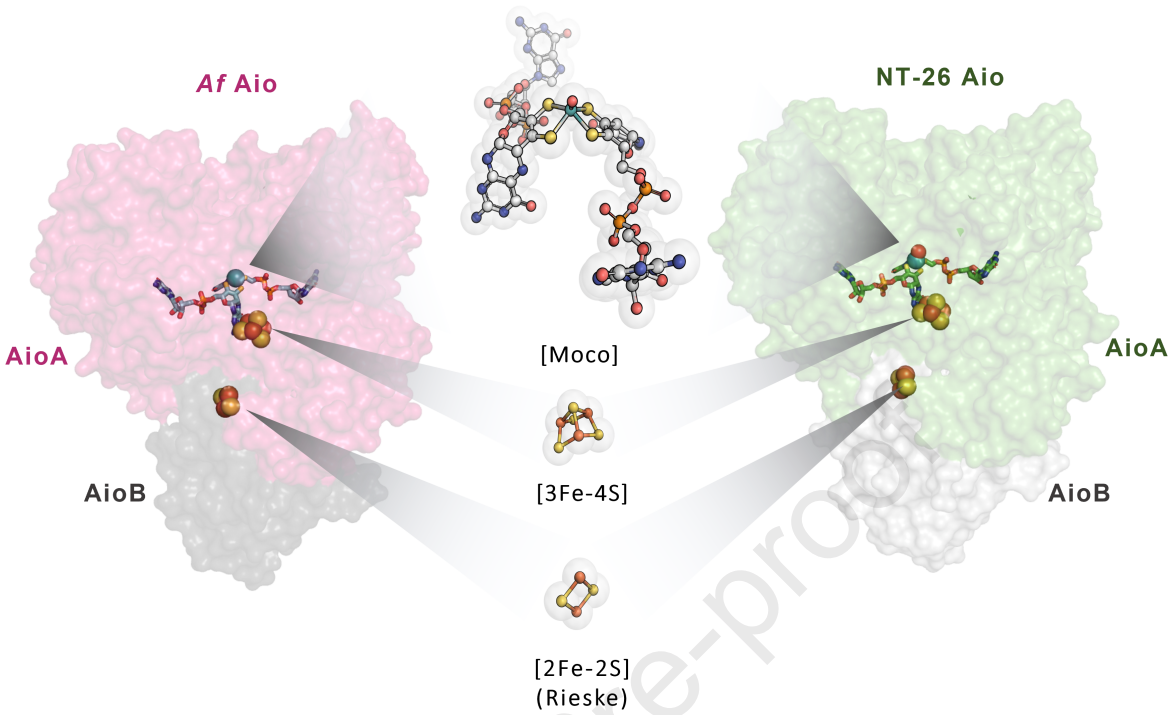

Journal Pre-proof

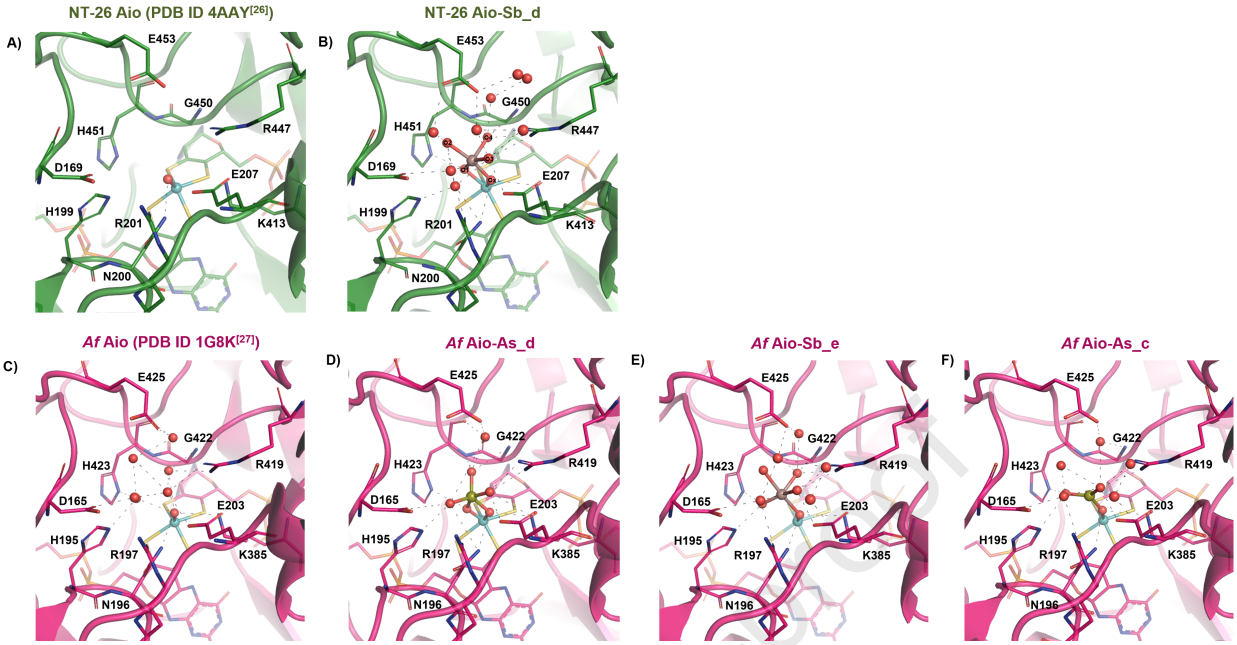

Journal Pre-proof

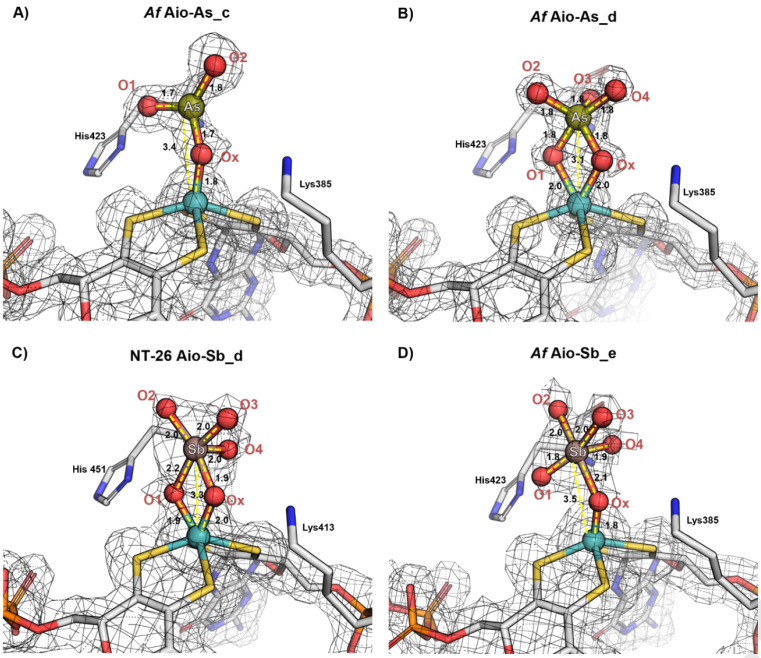

Journal Pre-proof

Journal Pre-proof

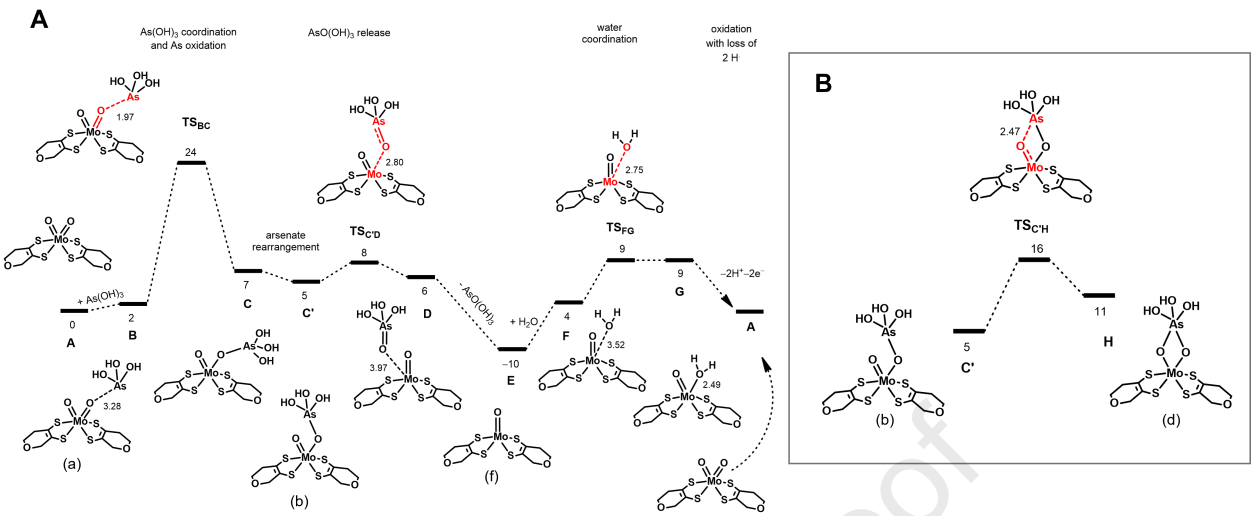

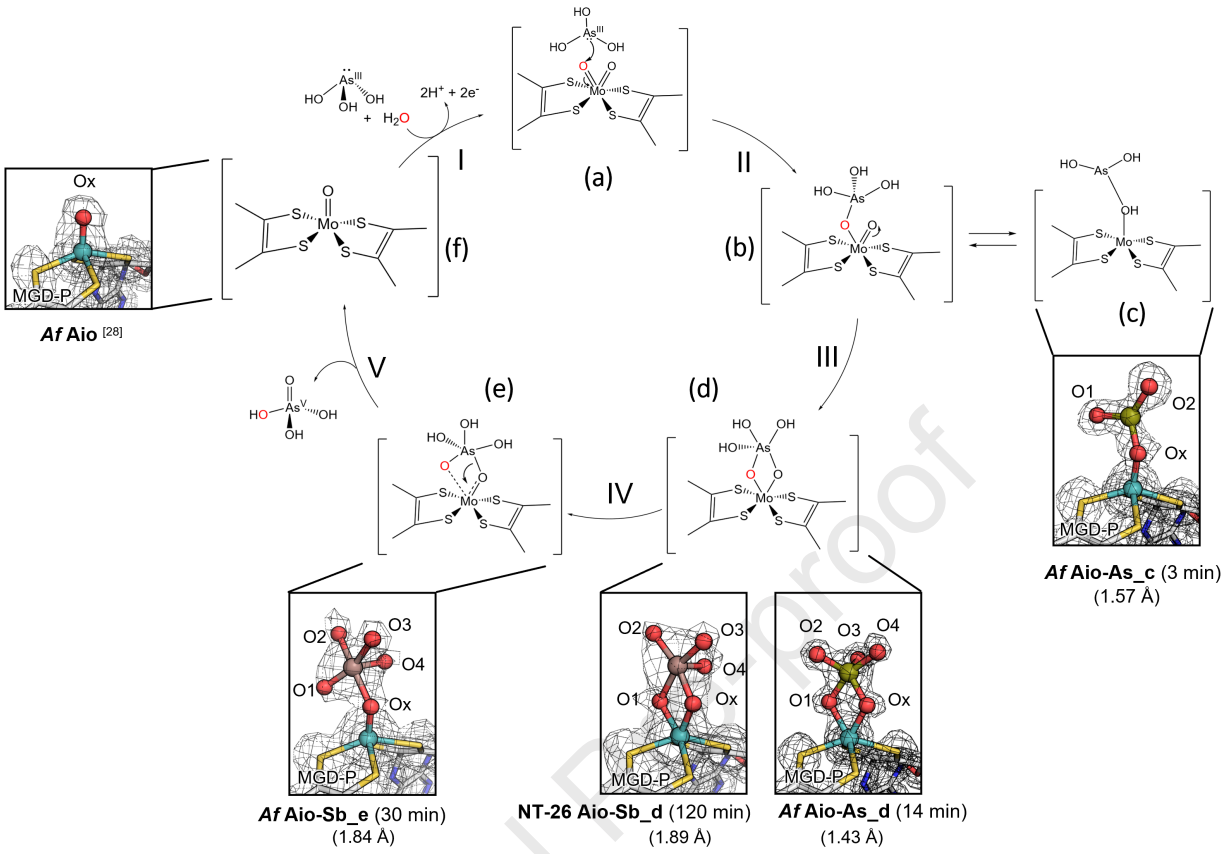

Journal Pre-proof